Journal of Alloys and Compounds 831 (2020) 154797

Contents lists available at ScienceDirect

Journal of Alloys and Compounds

journal homepage: http://www.elsevier.com/locate/jalcom

Synthesis and up-conversion of core/shell SrF_2:Yb^{3+},Er^{3+}@SrF_2:Yb^{3+},Nd^{3+} nanoparticles under 808, 975, and 1532 nm excitation wavelengths

Dominika Przybylska , Tomasz Grzyb *

Adam Mickiewicz University in Poznań, Faculty of Chemistry, Department of Rare Earths, Uniwersytetu Poznańskiego 8, 61-614, Poznań, Poland

ARTICLE INFO

Article history:
Received 15 January 2020
Received in revised form
18 February 2020
Accepted 14 March 2020
Available online 16 March 2020

Keywords:
Strontium fluoride
Luminescence
Down-conversion
Biological windows
Dual-range emission
Hydrothermal method

ABSTRACT

Sensitization of nanoparticles (NPs) by appropriate lanthanide ions is crucial for the obtained spectroscopic properties. Nd^{3+} ions can absorb light at around 808 nm, allowing for deep tissue imaging, Yb^{3+} ions can be effectively excited by 975 nm radiation which is utilized in many areas, e.g. in anti-counterfeit applications, while Er^{3+} ions are capable of absorption around 1532 nm, which in turn, is important for solar energy conversion. Here, we describe a method for Nd^{3+} and Er^{3+} ions isolation in NPs by the synthesis of core/shell structures. As an alternative to the most commonly used core/shell thermal decomposition synthesis procedures, our products were obtained in water by a hydrothermal method. SrF_2:Yb^{3+},Er^{3+}@SrF_2:Yb^{3+},Nd^{3+} NPs with sizes between 30 and 60 nm showed intense green to yellowish-red luminescence in the visible range, due to Er^{3+}-doping. Yb^{3+} played the role of bridging ions, transferring energy absorbed by Nd^{3+} ions between the shell and core phases, limiting, in the same way, cross-relaxation between Nd^{3+} sensitizer ions and Er^{3+} luminescence centers. Structure, morphology and spectroscopic properties were investigated, revealing interesting processes taking place in the prepared NPs.

1. Introduction

Studies of the up-conversion phenomenon (UC), initiated by the theoretical proposal of Bloembergen in 1951 [1] and proved experimentally by Auzel in 1966 [2], have significantly influenced materials science. Especially in nanotechnology, the UC has raised the important property of nanoparticles (NPs) allowing their applications in nanomedicine for cancer treatment and diagnosis [3–8]. The unique nature of UC has also been utilized in 3D displays, solar cells, lasers and fiber amplifiers, security markers, forensic science and pressure or temperature sensors [9–15].

UC is characterized by the conversion of low energy photons, from the near-infrared range, (NIR) to higher energy ones through the multiphoton absorption process [16], while down-conversion (DC) is the conversion of higher-energy photons to photons with lower energy (also known as down-shifting) [17]. Excellent materials which exhibit UC, as well as DC, are host compounds doped with lanthanide ions (Ln^{3+}). These ions, together with Sc^{3+} and Y^{3+} form a group of rare earth ions (RE^{3+}). Ln^{3+} ions have unique physicochemical and optical properties, due to their 4f electronic configuration. The energy levels of Ln^{3+} ions are well-defined, due to the effective shielding of the 4f orbitals caused by the filled 5s and 5p orbitals, and lie in the range of UV to NIR. Therefore, transitions within 4f subshell are relatively insensitive to the outer environment. As a result, materials doped with Ln^{3+} ions are efficient luminophores and usually show sharp emission spectra, long luminescence lifetimes, and large Stoke's shifts [18–20].

The most popular dopants used for UC are Yb^{3+}, Er^{3+}, Tm^{3+}, and Ho^{3+} ions. To enhance luminescence, Yb^{3+} ions usually play the role of sensitizers, due to their simple configuration of energy levels and large absorption cross-section between 900 and 1000 nm [21]. Energy absorbed by Yb^{3+} ions can be transferred to other Ln^{3+} ions resulting in their luminescence. This fact, and the existence of the so-called "first optical transparency window" in the range of 700–1000 nm [22], has been utilized in nanomedicine for optical imaging, drug delivery, and photothermal therapy [23]. However, NIR radiation with a wavelength of 980 nm is absorbed by water, which at higher power densities, may lead to the cell overheating effect [24]. The solution for this problem is the addition of Nd^{3+}

* Corresponding author.
E-mail address: tgrzyb@amu.edu.pl (T. Grzyb).

https://doi.org/10.1016/j.jallcom.2020.154797
0925-8388/

ions to the structure of NPs, as sensitizers for NIR radiation at 808 nm [25]. The water absorption coefficient is much lower at 808 nm, which also improves tissue penetrability [26]. Furthermore, the absorption cross-section of Nd^{3+} around 800 nm is significantly higher than Yb^{3+} around 980 nm.

Recently, UC of NPs under 808 nm has been intensively studied, mainly in triple-doped systems with Nd^{3+} ions used as sensitizers, and Yb^{3+} transferring absorbed energy to luminescence centers, usually Ho^{3+}, Er^{3+}, Tm^{3+}, or Tb^{3+} ions [27–33]. Because of the electronic structure of Nd^{3+} and the above-mentioned luminescent Ln^{3+} ions, a cross-relaxation (CR) process may occur, effectively quenching the luminescence of NPs. Hence, the concentration of Nd^{3+} is usually very low (below 2–3%) when all types of ions are in the same phase, which, in turn, results in low absorption at 808 nm [34–36]. To overcome this problem a few possibilities are available. The most developed solution for avoiding the CR process is the synthesis of core/shell or multi-shell NPs, combining NPs with organic dyes and surface plasmon coupling [29,37,38]. The first method, especially, is very promising. Shell layer not only increases the distance between the sensitizing and luminescent ions, which reduces the quenching process but also introduces isolation from the surrounding environment. Synthesis of core/shell NPs allows for the manipulation of the dopant's composition which can be used to obtain the desired emission and excitation properties. There are numerous examples of the utilization of core/shell structure of NPs: enhancement of UC quantum yield [39], tunable emission color, dual-mode emission from NIR to UV–Vis or to NIR with a longer wavelength than excitation light [40,41], multifunctionality of NPs through the addition of Gd^{3+} or Mn^{2+} ions [42], conjugation to biomolecules, drug delivery systems [43–46], and many others.

The main synthesis method of the core/shell NPs is the thermal decomposition, or precipitation, in high boiling-point solvents such as octadecene, oleic acid, or oleylamine, which forces the synthesis to be conducted at high temperature and under neutral gas protection [47]. The synthesis is complicated, has many steps, and the obtained products are hydrophobic which require additional procedures to remove oleic acid and octadecene from the NPs surface [27,34,48,49]. An alternative method which can be adopted for the preparation of core/shell NPs is solvothermal synthesis. The overall process is usually conducted in ethanol, oleic acid, ethylene glycol, or water, under high pressure and temperature, in special types of autoclaves [50–52].

The most environmentally friendly is the solvothermal synthesis with the use of water as a solvent: the hydrothermal method, very common for obtaining simple UC fluorides [53–56].

In the case of core/shell hydrothermal synthesis, just a few reports have been published (see Table S1 for more details). The first article, by Zazoni et al. where SrF_2:Yb^{3+}@SrF_2:Yb^{3+},Tm^{3+} UCNPs were obtained, was published in 2016 [57]. Shortly after, Li et al. reported on the hydrothermal synthesis of SrF_2:Yb^{3+},Tm^{3+}@CaF_2:Gd^{3+} NPs with magnetic properties [58]. In 2017 Alkahtani et al. presented a way of preparing YVO_4: Er^{3+}; Yb^{3+}@ YVO_4:Yb^{3+},Nd^{3+} NPs by precipitation in hydrothermal conditions [24]. Doping NPs with Nd^{3+} allowed authors to study UC under 808 nm excitation. Another study was reported by Cortelletti et al., in 2018 [59], where, during a fourth-step hydrothermal synthesis, SrF_2 NPs with a multi-shelled architecture were obtained. This complicated structure was tested as an NIR-activated nanothermometer.

Most papers referring to the hydrothermal synthesis of core/shell are based on the SrF_2 compound. This matrix is thermally stable also in high temperature and phase transition is not observed, which is important for light source applications [60]. Furthermore, strontium fluoride has low phonon energy (similar to $NaYF_4$) and high thermal conductivity [61]. What is more, SrF_2 doped with Yb^{3+} and Tm^{3+} shows better emission than prepared in the same way α-$NaYF_4$ about a similar size, which is known as one from the best UC materials [62]. Not without significance is the high value of quantum yield for SrF_2:Yb^{3+},Er^{3+} (2.8%), important for further applications [63]. In comparison to $NaREF_4$ (RE = rare earth element) NPs, the most often studied as hosts for 808/980 nm excited UC, SrF_2 NPs can be easily synthesized by the hydrothermal method. Synthesis of $NaREF_4$-type core/shell NPs was reported only twice and they were obtained only by solvothermal method (see Table S1) [64,65]. Usually, $NaREF_4$ materials, prepared via hydrothermal method are comprised of microsized crystals rather than nanocrystals [66–68].

Despite existing research on hydrothermal core/shell synthesis, obtaining high-quality NPs during the process conducted in water is still challenging. The possibilities of an optimized synthesis route, as well as morphology and spectroscopic properties improvement, have to be considered. Especially, the mechanism of UC in core/shell systems excited by Nd^{3+} ions should be carefully examined. In this article, SrF_2:Yb^{3+},Er^{3+}@SrF_2:Yb^{3+},Nd^{3+} core/shell NPs were prepared by a two-step hydrothermal synthesis in the presence of sodium citrate. In the described approach, the core/shell structure was proved spectroscopically by analysis of Nd^{3+} and Er^{3+} interactions. Furthermore, in our NPs, the chosen doping ions allowed for the excitation by three laser wavelengths: 808, 975, and 1532 nm, as well as luminescence in the Vis or NIR range. The obtained properties are promising for theranostics due to the emission from, and within, biological windows, as well as for energy conversion purposes highly demanded in solar cell development.

2. Methods

2.1. Materials

Lanthanide oxides: Er_2O_3 and Yb_2O_3, Nd_2O_3, (99.99%, Stanford Materials, United States) were dissolved separately in hydrochloric acid, HCl (ultra-pure, Sigma-Aldrich, 37%, Poland), in order to obtain the respective rare earth chloride solutions in a concentration of 1 or 0.25 M. Ammonium fluoride, NH_4F (98+%, Sigma-Aldrich, Poland), was used as the source of fluoride ions. Strontium chloride hexahydrate $SrCl_2 \cdot 6H_2O$ (Sigma-Aldrich, 99+%, Poland), citric acid trisodium salt dihydrate, NaCit (Sigma-Aldrich, 97%, Poland) were used as received, without further purification. Deionized water was used for the synthesis.

2.2. Synthesis of core SrF_2:Yb^{3+},Er^{3+} nanoparticles

To obtain 2 mmol of SrF_2 NPs, doped with 20% Yb^{3+} and 1% Er^{3+} ions, 1.58 mL of 1 M $SrCl_2$ solution and $YbCl_3$ mixed with $ErCl_3$ (0.40 mL of 1 M $YbCl_3$ and 0.08 mL of 0.25 M $ErCl_3$) were added to 20 mL of 1 M NaCit solution (anti-agglomeration and complexing agent). Then, 5 mL of 2.40 M solution of NH_4F (3 × excess in comparison to the stoichiometric amount) was added to the solution containing $SrCl_2$ and $LnCl_3$ salts. The pH of the final mixture was equal to 7.5. The as-prepared transparent solution was transferred into a 100 mL Teflon-lined vessel and hydrothermally treated for 24 h (200 °C, 15 bars and mixed), in an externally heated autoclave (Berghof BR-100). When the reaction was completed, the obtained white precipitate was purified by centrifugation and rinsed several times with water and ethanol. For the synthesis of core/shell structures, the wet product was re-dispersed in water and 5 mL of the formed colloid was transferred to a clean Teflon-lined vessel for the next step.

The presented description was the basic synthesis method. SrF_2 NPs were also prepared via modification of the above-mentioned

procedure, i.e. for a higher amount of product (5 mmol), shorter time of reaction (12 h), or with smaller excess of NH_4F reagent (2 ×). The modifications are included in the names of the samples used in this article, in brackets, and presented in Table 1.

2.3. Synthesis of core/shell $SrF_2:Yb^{3+},Er^{3+}@SrF_2:Yb^{3+},Nd^{3+}$ nanoparticles

$SrF_2:Yb^{3+},Er^{3+}$core NPs were coated by $SrF_2:Yb^{3+},Nd^{3+}$ shell via a second step in hydrothermal conditions. In a typical procedure, to obtain 2 mmol of shell containing 20% Yb^{3+} and 10% of Nd^{3+} ions, 1.40 mL of 1 M $SrCl_2$ solution and $YbCl_3$, mixed with $NdCl_3$ (0.40 mL of 1 M $YbCl_3$ and 0.80 mL of 0.25 M $NdCl_3$), were added to 20 mL of 1 M NaCit solution. Then, 5 mL of 2.4 M solution of NH_4F (3 × excess in comparison to the stoichiometric amount) was added to the solution containing $SrCl_2$ and $LnCl_3$ salts. The pH of the final mixture was equal to 7.5. The as-prepared transparent solution was transferred into the 100 mL Teflon-lined vessel, where the earlier core suspension was placed, and hydrothermally treated for 24 h (200 °C, 15 bars with mixing). When the reaction was completed, the obtained white precipitate was purified by centrifugation and rinsed several times with water and ethanol. The final product was dried under ambient conditions. A scheme of the synthesis procedure is presented in Fig. 1.

From the prepared samples, the two best emitting NPs were chosen to present their properties (SrF_2:20%Yb^{3+},1%Er^{3+}@SrF_2:20% Yb^{3+},10%Nd^{3+}, 5 mmol/5 mmol of $LnCl_3$, 24 h/24 h; SrF_2:20% Yb^{3+},1%Er^{3+}@SrF_2:20%Yb^{3+},10%Nd^{3+}, 2 mmol/2 mmol of $LnCl_3$, 24 h/12 h). Additionally, a core sample (SrF_2:20%Yb^{3+},1%Er^{3+},10% Nd^{3+}, 2 mmol/2 mmol of $LnCl_3$, 24 h) was prepared as a reference using the same composition of reactants and synthesis conditions as in the base procedure. This core sample was used to compare the morphology and spectroscopic properties of the triple-doped core (Yb^{3+}, Er^{3+}, Nd^{3+}) and core/shell where Nd^{3+} is separated from the activator ions and placed in the shell. To simplified naming of samples, all are presented in the above Table 1. Furthermore, different synthesis conditions are included in brackets in the sample name. The other core/shell samples, X-ray diffraction (XRD) patterns, dynamic light scattering (DLS), and zeta potential measurements, as well as spectroscopic properties, are attached in the Supplementary Materials.

2.4. Characterization

Powder diffractograms (XRD) were recorded on a Bruker AXS D8 Advance diffractometer in the Bragg-Brentano geometry, with Cu $K_{\alpha1}$ radiation, $\lambda = 1.5406$ Å, in the 2θ range from 10 to 60°. The reference data was taken from the International Centre for Diffraction Data (ICDD). The composition of the prepared materials was analyzed by Inductively Coupled Plasma Mass Spectrometer (ICP-MS) NexION 300D, PerkinElmer. Transmission-electron-microscopy (TEM) images were recorded on a Hitachi HT7700 with the voltage of 120 kV. Fourier transform infrared spectra (FT-IR) were recorded using a JASCO 4200 FT-IR spectrophotometer. DLS and zeta potential measurements were performed by using a Malvern Zetasizer Nano ZS instrument.

The luminescence characteristics (excitation, emission spectra, luminescence decay) of the prepared samples were measured on a QuantaMaster™ 40 spectrophotometer equipped with an Opolette 355LD UVDM tunable laser, with a repetition rate of 20 Hz, and a Hamamatsu R928 photomultiplier used as a detector for emission, excitation spectra, and decay times measurements. A CNI multi-wavelength 2W CW laser was used as the excitation source, coupled to a 200 μm optical fiber and collimator to determine dependencies between the emission intensity and laser power. As a detector, a Digital CCD Camera made by Princeton Instruments PIXIS:256E, equipped with an SP-2156 Imaging Spectrograph, was applied and corrected for the instrumental response.

3. Results and discussion

3.1. Structure and morphology

The prepared samples showed a single-phase structure with the $Fm\bar{3}m$ space group, for both the core (Fig. S1) and core/shell (Fig. 2 and S2). Depending on the conditions of the sample's preparation (higher amount of product or reaction time), particles of different sizes were obtained, as indicated by the widths of the XRD peaks. Furthermore, the shift of diffraction peaks towards a higher angle, in comparison to the reference pattern (ICDD, 01-086-2418, SrF_2), confirmed that Ln^{3+} ion doping into the host structure decreased the cell volume. This was caused by the smaller ionic radii of Yb^{3+}, Er^{3+}, and Nd^{3+}, compared to the Sr^{2+} ions ($rSr^{2+} = 1.26$ Å, $rNd^{3+} = 1.1090$ Å, $rEr^{3+} = 1.004$ Å, $rYb^{3+} = 0.985$ Å for coordination number CN = 8) [69]. Replacement of Sr^{2+} by Ln^{3+} ions, made structure of our products similar to $Sr_{0.84}Lu_{0.16}F_{2.16}$ reported in ICDD reference No. 01-082-0640, where $V = 186.27$ Å, whereas pure SrF_2 have cell volume, $V = 195.11$ Å^3.

To determine the size of the obtained compounds, three techniques were used: TEM, calculations via Scherrer's equation from XRD and DLS measurements (Table 2, S2 and Figs. 2 and 3, S1-S5).

Comparing the size of the core and core/shell NPs, calculated from Scherer's equation, the growth of particles is observed for both samples. The smaller size of the core, as well as the core/shell, had NPs synthesized in a shorter time and with a lower amount of precursors. The increase in size is similar for both samples (10 nm).

Table 1
List of samples described in this article.

Sample name	Core 1st step				Core/shell 2nd step			
	Amount of precursor (mmol)	Excess of NH_4F	Reaction time (h)	Other	Amount of precursor (mmol)	Excess of NH_4F	Reaction time (h)	Other
Base procedure: 20%Yb^{3+},1%Er^{3+}@20% Yb^{3+},10%Nd^{3+}	2	3	24		2	3	24	–
20%Yb^{3+},1%Er^{3+}@20%Yb^{3+},10%Nd^{3+} (5 mmol/ 5 mmol)	5	3	24	–	5	3	24	–
20%Yb^{3+},1%Er^{3+}@20%Yb^{3+},10%Nd^{3+} (24 h/ 12 h)	2	3	24	–	2	3	12	–
20%Yb^{3+},1%Er^{3+}@20%Yb^{3+},20%Nd^{3+} (2 × NH_4F/2 × NH_4F)	2	2	24	–	2	2	24	20% Nd^{3+}
20%Yb^{3+},1%Er^{3+}@20%Yb^{3+},10%Nd^{3+} (12 h/ 24 h)	2	3	12	–	2	3	24	–
20%Yb^{3+},1%Er^{3+},10%Nd^{3+}	2	3	24	–	–	–	–	–

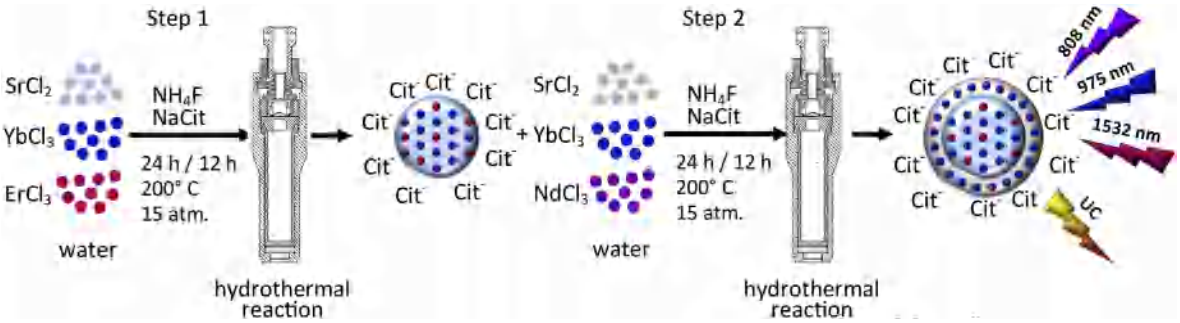

Fig. 1. Schematic representation of the synthesis procedure of SrF_2:Yb^{3+},Er^{3+}@SrF_2:Yb^{3+},Nd^{3+} core/shell NPs via a hydrothermal method.

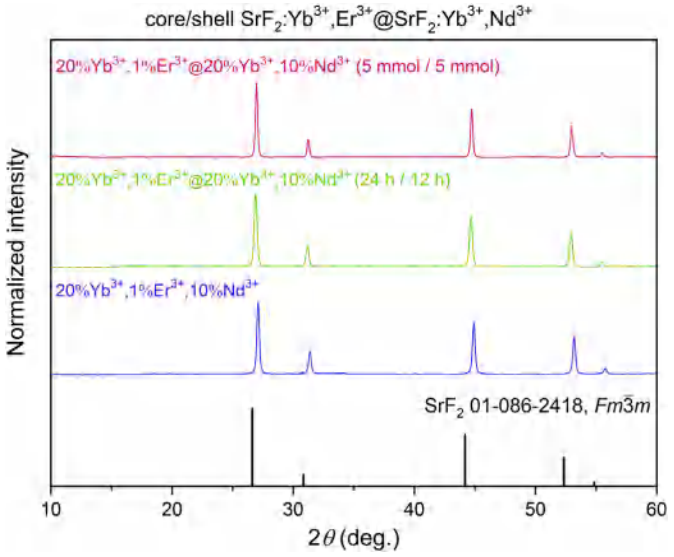

Fig. 2. XRD patterns of SrF_2 core/shell samples synthesized by hydrothermal method.

The DLS measurements confirmed the particle growth and revealed an additional tendency of the agglomeration of NPs.

The size of the presented NPs was also confirmed by analysis of TEM pictures for the core samples as well as for the core/shells (Figs. 3 and S5). The structure obtained from synthesis for 5 mmol of the product shows an irregular shape for both the core and core/shells, with sizes of 47 and 61 nm respectively. A reduction of the precursors' concentration and time of the 2nd step resulted in NPs with a more regular spherical shape and a lower size distribution (27 and 45 nm for core and core/shell, respectively).

To examine the surface of the particles, FT-IR spectra and zeta potentials were measured (for details see Fig. S6 and Table S3). The presence of citrate groups on the NPs surface was detected from the appearance of the signals assigned to the following types of vibrations: −OH stretching vibration (3457 cm^{-1}), −CH asymmetric and symmetric stretching vibrations (2962 and 2840 cm^{-1}), −C═O stretching vibrations (1622 cm^{-1}) and −CH scissoring (1400 cm^{-1}). Furthermore, there was no significant shift in signals between the core and core/shell samples which indicates the lack of impact of the second step of synthesis on the surface of the nanoparticles. Moreover, samples exhibited a negative charge on the surface and usually, the cores had a higher negative charge than the core/shells, from −28.6 mV to −20.7 mV, and from −20.6 mV to −16.7 mV, respectively. The small difference between the presented values confirms similar stability in water of the prepared cores and core/shells structures and their tendency to agglomerate due to a not very high potential. Furthermore, an additional amount of Ln^{3+} ions in the structure of NPs can reduce the negative charge of NPs. Also, the growth of NPs can influence their charge, which may be responsible for observed differences between core and core/shells as electrostatic interaction between NPs decrease [71]. However, for a few samples differences between zeta potentials for core and core/shell are within the margin of measurement error.

It is very important to properly determine the elemental composition of the obtained products and confirm the core/shell structure. The existence of a core/shell structure can be assumed by the observed increase in the size of NPs after 2nd step of the synthesis, which is shown in Table 2 and S2. However, quantitative elemental analysis of the core/shell structures is difficult [27]. In this work, the ICP-MS technique was used for this purpose (see Table S4 for details). This method confirmed the coexistence of Sr^{2+}, Nd^{3+}, Er^{3+}, Yb^{3+}, and F^- ions in all the core/shell samples with only a slight difference between them.

3.2. Spectroscopic properties

To investigate the spectroscopic properties of the synthesized NPs, their excitation and emission spectra, as well as chromaticity diagrams, decay times and dependence of luminescence intensity on laser power were measured. Analysis of UC and DC properties is the most reliable method to confirm the successful doping with Ln^{3+} ions and the formation of the core/shell structure. In Fig. 4a excitation spectra of two the best emitting samples are presented together with the triple-doped core sample. In the spectra, several

Table 2
Sizes of obtained NPs, calculated from the Scherrer's equation based on XRD analysis [70], hydrodynamic diameters determined by DLS measurements, and NPs diameters taken from TEM images.

Sample	Scherrer equation (nm)		Hydrodynamic diameter (nm)		TEM images (nm)	
	Core	Core/shell	Core	Core/shell	Core	Core/shell
20%Yb^{3+},1%Er^{3+}@20%Yb^{3+},10%Nd^{3+} (5 mmol/5 mmol)	49.2 ± 0.6	59.3 ± 0.9	76.9 ± 27.3	230.4 ± 93.0	47.1 ± 9.8	60.5 ± 12.3
20%Yb^{3+},1%Er^{3+}@20%Yb^{3+},10%Nd^{3+} (24 h/12 h)	30.9 ± 0.9	41.9 ± 0.4	68.6 ± 20.3	158.7 ± 59.2	26.6 ± 4.3	45.3 ± 8.5
20%Yb^{3+},1%Er^{3+},10%Nd^{3+}	35.6 ± 0.3	–	84.2 ± 29.5	–	34.7 ± 8.4	–

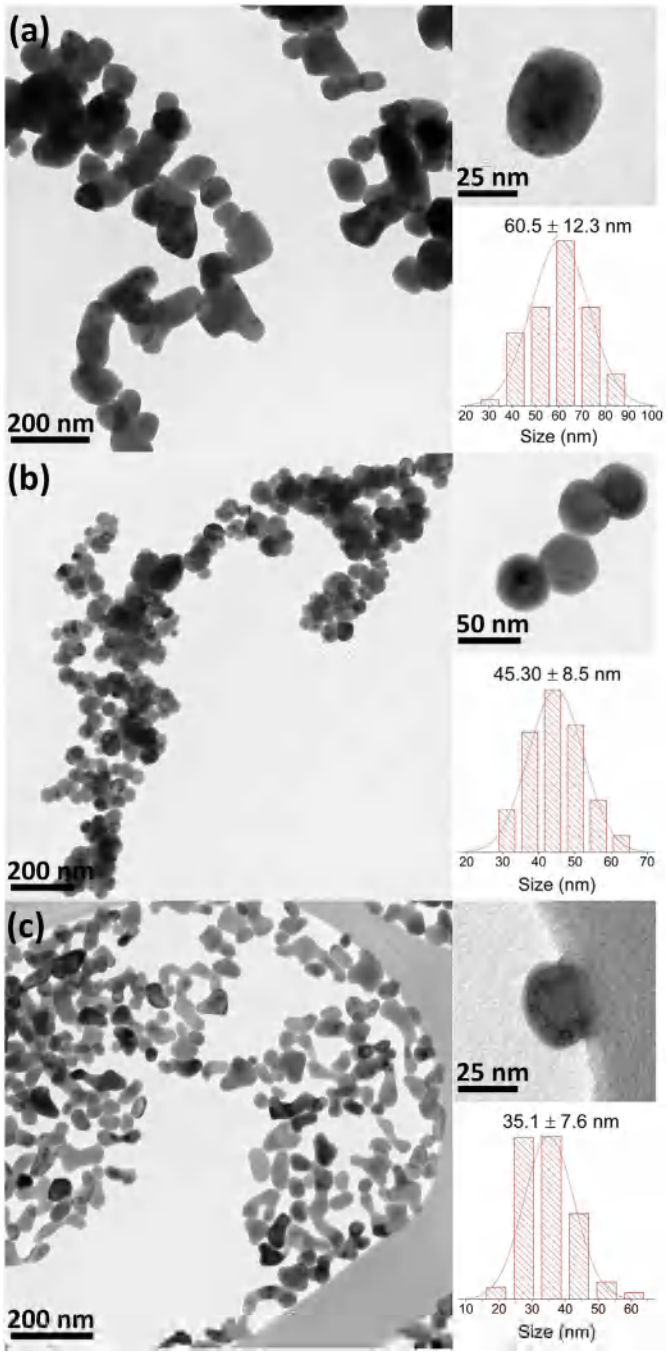

Fig. 3. TEM pictures and NPs size distributions of hydrothermally synthesized (a) SrF_2:20%Yb^{3+},1%Er^{3+}@SrF_2:20%Yb^{3+},10%Nd^{3+} (5 mmol/5 mmol), (b) SrF_2:20%Yb^{3+},1% Er^{3+}@SrF_2:20%Yb^{3+},10%Nd^{3+} (24 h/12 h), and (c) SrF_2:20%Yb^{3+},1%Er^{3+},10%Nd^{3+}.

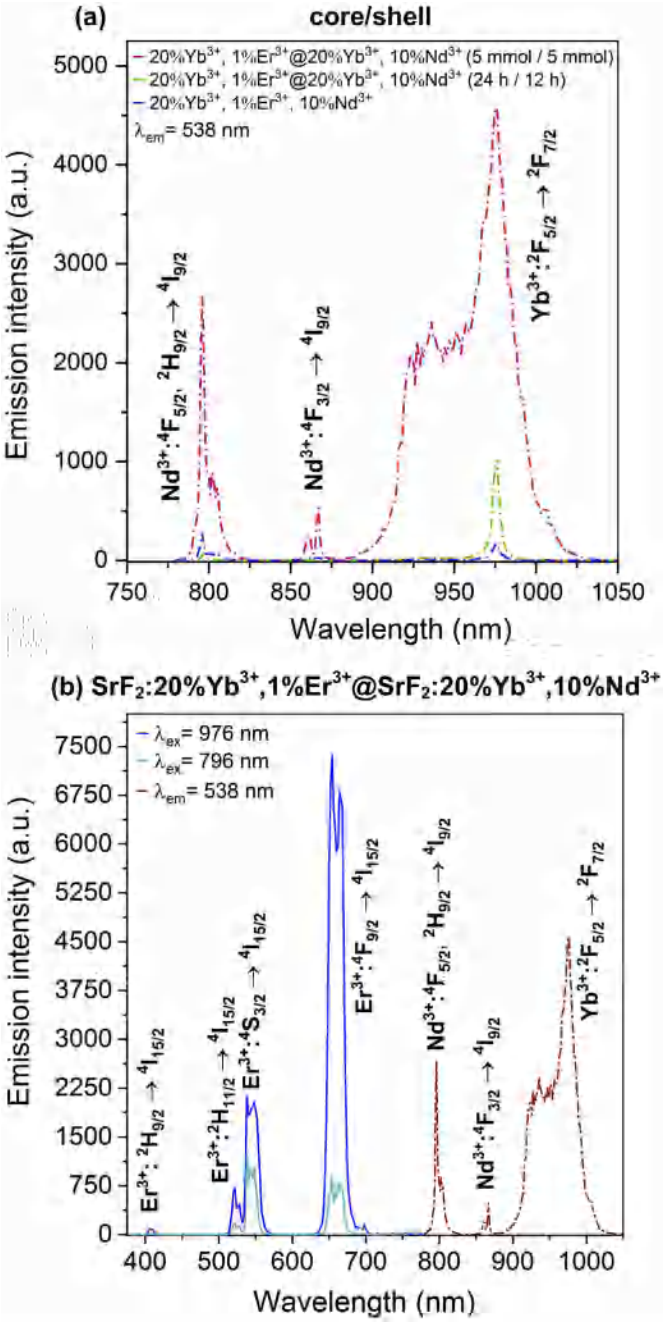

Fig. 4. (a) Excitation spectra of prepared samples and (b) emission spectra under different excitation wavelengths of SrF_2:20%Yb^{3+},1%Er^{3+}@SrF_2:20%Yb^{3+},10%Nd^{3+}, (5 mmol/5 mmol) sample. Spectra were obtained under pulsed excitation source (at 25 mJ cm^{-2}).

excitation bands are visible as a result of the presence of Yb^{3+} and Nd^{3+} ions. Four possible wavelengths can be used for the sample's excitation, i.e. 796, 802, and 866 nm, connected with Nd^{3+} transitions: $^2H_{9/2} \rightarrow {}^4I_{9/2}$, $^4F_{5/2} \rightarrow {}^4I_{9/2}$ and $^4F_{3/2} \rightarrow {}^4I_{9/2}$ respectively, or 976 nm as a result of $^4F_{5/2} \rightarrow {}^4F_{7/2}$ transition of Yb^{3+} ions. The sample SrF_2:20%Yb^{3+},1%Er^{3+}@SrF_2:20%Yb^{3+},10%Nd^{3+} prepared from 5 mmol of product, with 3 × excess of NH_4F during 24 h synthesis (1st and 2nd step), shows a higher emission and excitation intensity than the others. What is more, the strongest excitation band was registered for $^4F_{5/2} \rightarrow {}^4F_{7/2}$ transition of Yb^{3+} ions, which is consistent with the highest emission intensity under 976 nm excitation (Fig. 4b). However, the emission under 796 nm excitation is also relatively intense. The difference between the emission intensities through excitation by Yb^{3+} ions and Nd^{3+} can be as a result of the quenching of Er^{3+} ions due to back energy transfer ($Nd^{3+} \rightarrow Yb^{3+} \rightarrow Er^{3+} \rightarrow Nd^{3+}$) [72]. It is worth noting that after the 2nd step of the synthesis, a significant enhancement of luminescence was obtained (see Figs. S7 and S8) due to the protective shell covering, which is characteristic for core/shell structures.

Emission spectra were also measured using a continuous laser as an excitation source (808, 975, and 1532 nm wavelengths) which

are presented in Fig. 5 and S9. From all excitation wavelengths, the highest UC emission was measured under 975 nm excitation. Furthermore, from the core, as well as core/shell samples, the sample prepared for 5 mmol of product in the 1st and 2nd step of synthesis showed the brightest emission when 975 nm wavelength was used, which results from the largest NPs and hence, a lower surface-related quenching.

The most visible difference between the core and core/shell NPs is shown in Fig. 5c where the separation of Nd^{3+} ions from the core allowed for an almost 15 times higher emission intensity under 808 nm excitation than that for the bare analogs, in which all dopant ions are in the same phase. The registered quenching effect in the triple-doped NPs is very strong and can be as a result of the high concentration of Nd^{3+} ions. Hence, the shortened distance between the sensitizer and luminescent ions leads to cross-relaxation between lanthanide ions. The unfavorable effect of triple-doping is visible in all the measured spectra presented in Fig. 5a–c. These results confirmed the sense and advantages of the synthesis of core/shell structures for applications in 808 nm sensitized UC.

Based on the collected emission spectra, the better emission properties under 975 nm excitation can be obtained during the synthesis of 5 mmol of the reaction product, 3 × excess of NH_4F, and 24 h of reaction for the core and core/shell NPs. However, under 808 nm excitation wavelength, the sample obtained from 2 mmol of product and 2 × excess of NH_4F for the core and core/shell synthesis, where the time of 1st step is 24 h and 2nd is 12 h, shows a more effective emission in the visible region than the above-mentioned sample.

The prepared samples also showed a DC phenomenon under 808 nm or 975 nm excitation wavelengths (Fig. 5d and e, S10). As a result, the emission of Yb^{3+} and Er^{3+} in the NIR region (second, 1000–1400 nm, and third biological window, 1500–1700 nm) [33,73] was detected. What is interesting, the strongest luminescence of Er^{3+} ions under 975 nm excitation was observed for core samples, ($^4I_{13/2} \rightarrow {}^4I_{15/2}$ transition). A lower luminescence of Er^{3+} ions in the NIR range for core/shell NPs indicates two effects: a more probable radiative relaxation of Er^{3+} ions from higher energy levels ($^2H_{9/2}$, $^2H_{11/2}$, $^4S_{3/2}$, $^4F_{9/2}$), and a lower concentration of Er^{3+} ions in the volume of measured powdered sample as a result of the addition of shell to core NPs. The emission of Yb^{3+} ions under 975 nm excitation is very similar for both the core as well as the core/shell sample. Excitation with 808 nm also resulted in the emission of Er^{3+} as an effect of the energy migration process. Because Er^{3+} ions can also absorb light at 808 nm due to $^4I_{15/2} \rightarrow {}^4I_{9/2}$ transition, core NPs, doped only with Yb^{3+} and Er^{3+}, showed weak emission under 808 nm laser radiation. However, the presence of Nd^{3+} ions in the shell significantly increased the emission at around 1525 nm associated with Er^{3+} ions (Fig. 5d). When all of the Ln^{3+} ions are in the same phase, a weak emission

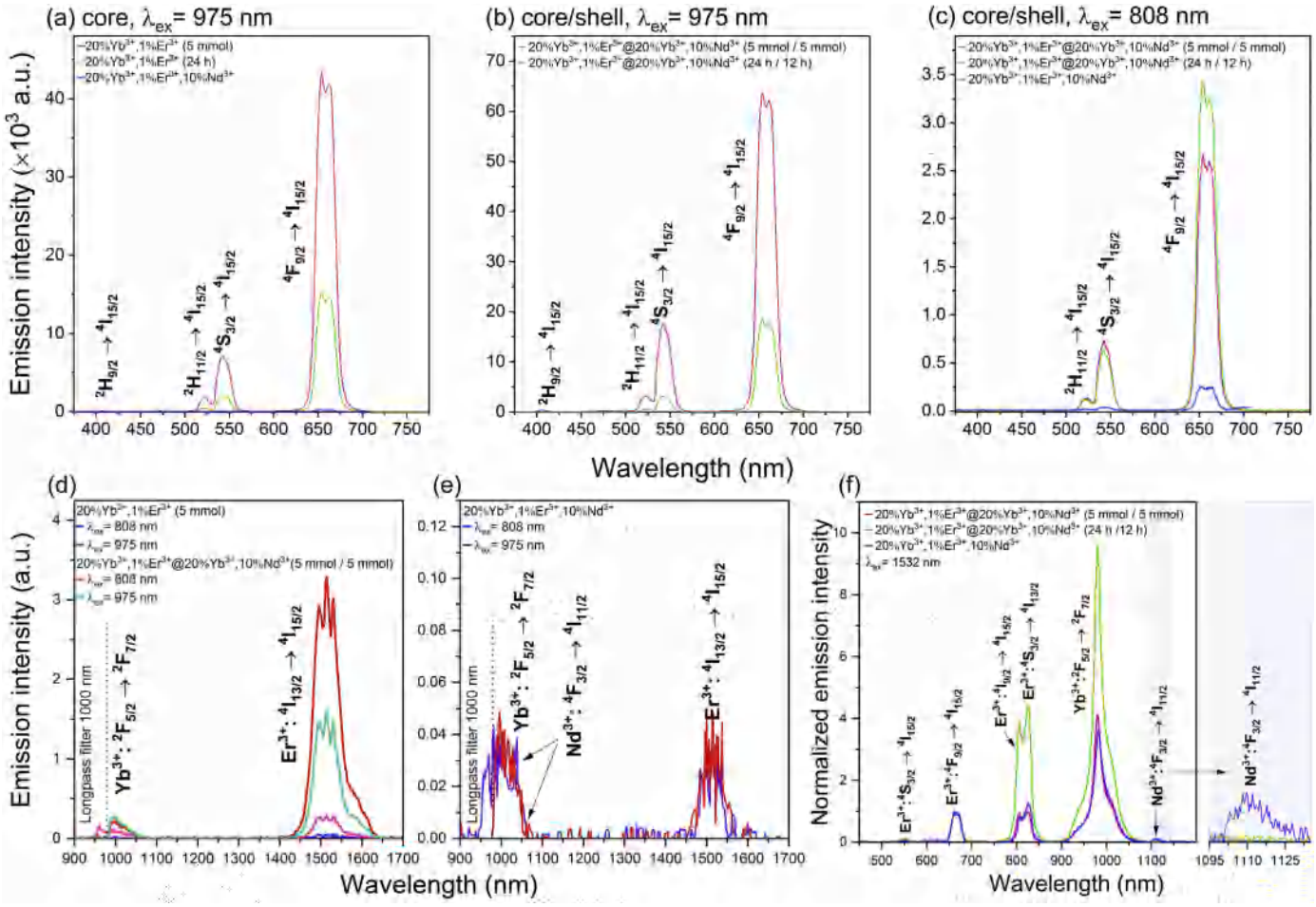

Fig. 5. (a–c) Up-conversion and (d,e) down-conversion emission of selected NPs (SrF_2:20%Yb^{3+},1%Er^{3+}@SrF_2:20%Yb^{3+},10%Nd^{3+}, (5 mmol/5 mmol) and SrF_2:20%Yb^{3+},1%Er^{3+},10% Nd^{3+}) sample in the Vis and NIR range under excitation with 808 or 975 nm CW laser light; (f) up-conversion luminescence of selected samples under excitation with 1532 nm CW laser light, normalized to $^4F_{9/2} \rightarrow {}^4I_{15/2}$ emission band of Er^{3+} ions. Laser powers: (a–c) 15 W cm^{-2} for 808 and 975 nm, (d, e) 22, 27, or 61 W cm^{-2} for 808, 975, and 1532 nm respectively.

from Nd^{3+} ions ($^4F_{3/2} \rightarrow {}^4I_{11/2}$) is also observed when 808 nm excitation is applied (Fig. 5e). The reason for such a result is the ineffective energy transfer to Er^{3+} ions resulting in a higher number of Nd^{3+} remaining in their excited state. The lack of energy migration to Er^{3+} ions through Yb^{3+} ions caused the radiative relaxation of Nd^{3+} ions with an associated luminescence (see Fig. 5e). In the core/shell structures, the back-energy transfer to Nd^{3+} ions is ineffective due to the separation of Nd^{3+} ions from Er^{3+} ions.

Up-conversion luminescence of prepared NPs was also observed under 1532 nm excitation (Fig. 5f). However, we utilized this excitation wavelength mainly to confirm the formation of core/shell structures. The applied laser wavelength is absorbed only by Er^{3+} ions through the $^4I_{15/2} \rightarrow {}^4I_{12/2}$ transition. Therefore, if cross-relaxation between Er^{3+} and Nd^{3+} occurs, emission from the latter one is observed. This process involves excitation of Er^{3+} to at least the $^4I_{9/2}$ level (absorption of two 1532 nm photons) and the energy transfer to $^2H_{9/2}$ excited state of the Nd^{3+} ions what is not possible through Yb^{3+} ions bridging the core and shell phases in core/shell NPs. The emission from Nd^{3+} ions around 1100 nm was only detected when all three Ln^{3+} dopants were present in a single core NPs (20% Yb^{3+}, 1% Er^{3+} and 10% Nd^{3+}). In the core/shell structures, the emission of Nd^{3+} was not observed which confirms the assumed structures.

The luminescence color of the prepared samples was dependent upon the excitation laser type (for chromaticity diagrams see Fig. S11 and ratios between luminescence bands in Fig. S12). Under a continuous excitation source with 808 and 975 nm, all samples exhibited a yellowish-orange emission with a small shift into the red region after covering core NPs with a shell. The use of pulsed laser as an excitation source resulted in green to orange emission of samples, depending on the synthesis conditions and concentration of dopant ions. Moreover, the use of 796 nm excitation light resulted in a green emission, whereas at 975 nm, this was yellowish-green as seen by the human eye. The result may indicate a different mechanism of Er^{3+} ion's excitation.

More information about the synthesized core/shell structures can be established based on emission lifetimes, calculated from decay time measurements (Fig. 6 and S13, Table 3, S4). It can be clearly seen that after shell covering, the lifetimes are longer than for the core particles. Extension of lifetimes is connected with the surface protective effect, minimizing quenching and decreasing the cross-relaxation processes between ions because of longer distances between them [49,74,75]. SrF_2:20%Yb^{3+},1%Er^{3+},10%Nd^{3+} NPs had a very short decay time which indicates, similar to the luminescence measurements, the quenching effect of Nd^{3+} ions due to the cross-relaxation process. Additionally, a higher concentration of Nd^{3+} in a shell (20%) quenches the luminescence intensity as well as decreases the lifetimes (SrF_2:20%Yb^{3+},1%Er^{3+}@SrF_2:20%Yb^{3+},20%Nd^{3+}, 2 × NH_4F/2 × NH_4F, Fig. S13, Table S4). Analogous lifetimes for prepared NPs were calculated for 808 nm excitation, confirming effective transfer between $Nd^{3+} \rightarrow Yb^{3+} \rightarrow Yb^{3+} \rightarrow Er^{3+}$ ions.

Important information about UC mechanism under 808 nm and 975 nm excitation, and the difference between them for prepared NPs, can be obtained from measurements of dependences of the luminescence intensity on the laser power. The number of photons can be estimated from the equation [76]:

$$I \propto P^n \quad (1)$$

where I is the UC intensity, P the pumping excitation power density, and n is the number of photons required to populate the excited state. The results of the calculations are collected in Table 4 (additionally Table S5 and for measurement results see Fig. S14).

Measurements have been distinguished by core and core/shell samples as well as the length of excitation wavelength (808 or 975 nm) and observed transitions. When we consider the two-photon excitation process of $^2H_{11/2}$, $^4S_{3/2}$, $^4F_{9/2}$, energy level, for samples doped with Yb^{3+} and Er^{3+}, the slope values are higher than one, which agrees with theoretical assumptions. An increase of slope value is especially observed for core/shell samples prepared from 5 mmol of precursors, under 975 nm excitation, in comparison to core ones. However, under 808 nm excitation, the slope coefficients have a lower value than under 975 nm excitation (from 0.81 to 1.89). The reason for this could be connected with energy transfer through intermediate Yb^{3+} ions, which has an influence on increasing the possibility of cross-relaxation occurring between ions, and the saturation effect, which is especially visible for the $^4F_{9/2} \rightarrow {}^4I_{15/2}$ transition. Furthermore, the triple-doped core sample has a significantly lower slope value than the other two samples. Additionally, for the sample prepared from 5 mmol of Ln^{3+} precursor (1st and 2nd step), the slope coefficient was also calculated for a three-photon process- $^2H_{9/2} \rightarrow {}^4I_{15/2}$ transition.

Based on the spectroscopic studies of synthesized NPs, the UC as well DC mechanisms are proposed for core/shell NPs in Fig. 7 (see Fig. S15 for a scheme of energy processes in core NPs). To observe UC emission, three different excitation wavelengths may be used. The first possibility of Er^{3+} ions excitation is the energy transfer from Yb^{3+} ions being excited by 975 nm laser radiation. This process is known as energy transfer up-conversion (ETU). All of the Yb^{3+} ions incorporated into the core, as well as the shell, can effectively absorb exciting radiation. When sensitizer ions are placed in the core, after excitation of Yb^{3+} ions to the $^2F_{5/2}$ energy level, energy is transferred directly to the $^4I_{11/2}$ excited state of Er^{3+} ions. Another possibility is the migration of energy between the core and shell phases among Yb^{3+} ions [77,78]. The second excitation pathway is possibly due to doping with Nd^{3+} ions which are capable of absorption of the 808 nm excitation radiation. After absorption of photons by Nd^{3+} ions and their excitation to the $^4F_{5/2}$ level, relaxation to $^4F_{3/2}$ occurs at the first step. Then, energy transfer to Er^{3+} ions is possible via Yb^{3+} ions, i.e. Nd^{3+}(shell)→Yb^{3+}(shell)→Yb^{3+}(core)→Er^{3+}(core). This process is known as energy migration up-conversion (EMU).

Another possibility is the direct excitation of Er^{3+} ions under 1532 nm laser light. As a result of photons absorption, excitation from the $^4I_{15/2}$ ground state of Er^{3+} ions to their $^4I_{13/2}$ excited state occurs (ground state absorption, GSA) and next, to higher excited states, yielding Er^{3+} in their $^2H_{11/2}$ excited state (excited state absorption, ESA). Furthermore, energy transfer from Er^{3+} to Yb^{3+} ions is possible resulting in the emission at around 980 nm.

Moreover, under 975 nm and 808 nm excitations, DC in the NIR region was registered for the core as well as for the core/shell structures. Similar to the UC, energy transfer between Yb^{3+} and Er^{3+} ions was responsible for the emission of Er^{3+} at around 1525 nm. Additionally, a partial back energy transfer from Yb^{3+} in the core, to Yb^{3+} in the shell, can be observed with the occurred luminescence (Yb^{3+}:$^2F_{5/2} \rightarrow {}^2F_{7/2}$). A similar process, through excitation under 808 nm by Nd^{3+} ions with mediated energy transfer ($Nd^{3+} \rightarrow Yb^{3+} \rightarrow Yb^{3+} \rightarrow Er^{3+}$), was also observed.

Additionally, for the prepared triple-doped core sample, (Nd^{3+}, Er^{3+}, Yb^{3+}) a mechanism for the energetic processes is proposed (Fig. S15). Hence, UC emission of Er^{3+} can be obtained under 808 nm, 975 nm, and 1532 nm excitation wavelengths. However, in this sample, a different mechanism of excitation via Nd^{3+} ions can occur. Energy can be directly transferred from Nd^{3+} to activator ions (Nd^{3+}:$^4F_{5/2} \rightarrow Er^{3+}$:$^4I_{11/2}$) or by energy migration transfer ($Nd^{3+} \rightarrow Yb^{3+} \rightarrow Er^{3+}$). Also, under direct excitation of Er^{3+} ions (λ_{ex} = 1532 nm), an additional emission from Nd^{3+} ions can be observed (Nd^{3+}:$^4F_{3/2} \rightarrow {}^4I_{11/2}$) as the result of energy transfer from

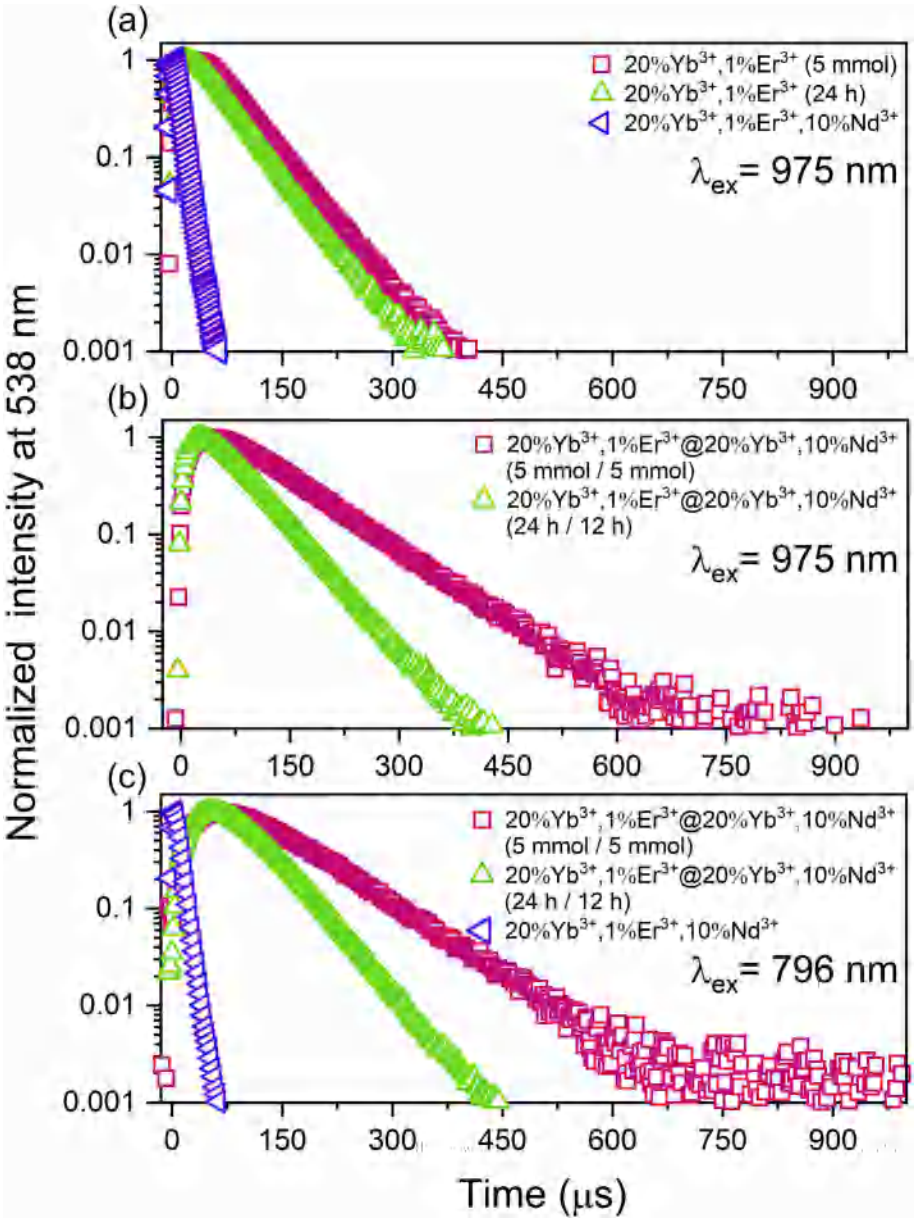

Fig. 6. Decay times of the two best emitting core/shell NPs, and the triple-doped sample for comparison, measured at 538 nm for the $^4S_{3/2} \rightarrow {}^4I_{15/2}$ transition of Er^{3+} ions, under pulsed excitation source (at 25 mJ cm^{-2}).

Table 3
Emission lifetimes calculated from the measured luminescence decays of core and core/shell samples under 796 nm or 976 nm pulsed laser excitations (at 25 mJ cm^{-2}) (for decays see Fig. S13, err <1.1 μs).

Sample	Lifetimes (μs)								
	core			core/shell					
	λ_{ex} = 975 nm			λ_{ex} = 975 nm			λ_{ex} = 796 nm		
	$^2H_{11/2} \rightarrow {}^4I_{15/2}$	$^4S_{3/2} \rightarrow {}^4I_{15/2}$	$^4F_{9/2} \rightarrow {}^4I_{15/2}$	$^2H_{11/2} \rightarrow {}^4I_{15/2}$	$^4S_{3/2} \rightarrow {}^4I_{15/2}$	$^4F_{9/2} \rightarrow {}^4I_{15/2}$	$^2H_{11/2} \rightarrow {}^4I_{15/2}$	$^4S_{3/2} \rightarrow {}^4I_{15/2}$	$^4F_{9/2} \rightarrow {}^4I_{15/2}$
$20\%Yb^{3+},1\%Er^{3+}@20\%Yb^{3+},10\%Nd^{3+}$ (5 mmol/ 5 mmol)	53	48	256	98	99	376	113	110	306
$20\%Yb^{3+},1\%Er^{3+}@20\%Yb^{3+},10\%Nd^{3+}$ (24 h/12 h)	47	49	245	60	64	250	66	67	217
$20\%Yb^{3+},1\%Er^{3+},10\%Nd^{3+}$	9	9	52	–	–	–	9	9	56

Table 4
The number of photons involved in the UC mechanism, determined from the dependences of luminescence intensity on laser power for core and core/shell NPs under 808 nm and 975 nm continuous laser excitation wavelengths (for experimental results see Fig. S14, err <0.05).

Sample	Number of photons											
	core				core/shell							
	λ_{ex} = 975 nm				λ_{ex} = 975 nm				λ_{ex} = 808 nm			
	$^2H_{9/2} \rightarrow {^4I_{15/2}}$	$^2H_{11/2} \rightarrow {^4I_{15/2}}$	$^4S_{3/2} \rightarrow {^4I_{15/2}}$	$^4F_{9/2} \rightarrow {^4I_{15/2}}$	$^2H_{9/2} \rightarrow {^4I_{15/2}}$	$^2H_{11/2} \rightarrow {^4I_{15/2}}$	$^4S_{3/2} \rightarrow {^4I_{15/2}}$	$^4F_{9/2} \rightarrow {^4I_{15/2}}$	$^2H_{9/2} \rightarrow {^4I_{15/2}}$	$^2H_{11/2} \rightarrow {^4I_{15/2}}$	$^4S_{3/2} \rightarrow {^4I_{15/2}}$	$^4F_{9/2} \rightarrow {^4I_{15/2}}$
20%Yb^{3+},1%Er^{3+}@20%Yb^{3+},10%Nd^{3+} (5 mmol/5 mmol)	0.96	1.64	1.29	1.35	2.41	2.12	1.88	2.89	0.81	1.60	1.37	1.89
20%Yb^{3+},1%Er^{3+}@20%Yb^{3+},10%Nd^{3+} (24 h/12 h)	–	2.21	2.08	2.08	1.96	2.22	2.05	2.02	–	1.64	1.35	1.52
20%Yb^{3+},1%Er^{3+},10%Nd^{3+}	–	0.62	0.72	1.48	–	–	–	–	–	1.14	0.84	1.03

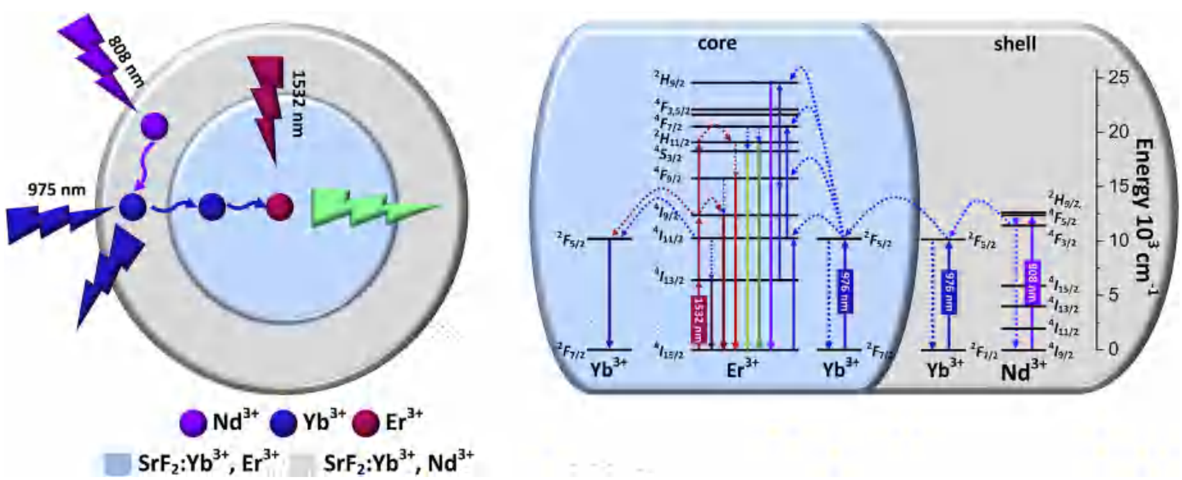

Fig. 7. Scheme of energetic processes taking place in for SrF_2: Yb^{3+}, Er^{3+}@SrF_2: Yb^{3+}, Nd^{3+} core/shell systems, under NIR excitation (λ_{ex} = 808, 975, or 1532 nm).

Er^{3+} to Nd^{3+} ions, which is neglected in the core/shell structures. However, due to the shortened distance between the sensitizer and activator, significant emission quenching and a strong cross-relaxation process were observed.

4. Conclusions

We have successfully synthesized SrF_2:Yb^{3+},Er^{3+}@SrF_2:Yb^{3+},Nd^{3+} core/shell NPs, by a two-step hydrothermal method. The synthesis procedure was optimized considering the spectroscopic properties as well as the morphology of NPs. The effects of different variables, such as the amount of precursors or time of reaction, were investigated. The developed procedure allowed for the synthesis of small, single-phase NPs with sizes between 30 and 60 nm, depending on the synthesis conditions. NPs formed stable water colloids with negatively charged surfaces, and hydrodynamic diameters between 80 and 230 nm. Intense emission under 808, 975, and 1532 nm was observed in the visible as well as NIR range (up- and down-conversion). The processes taking place in the core/shell structures were investigated by measuring excitation and emission spectra, power dependences, and luminescence decays under continuous or pulsed excitation sources. We have proved the existence of core/shell structures by selectively exciting Er^{3+} ions and the observation of cross-relaxation effects with Nd^{3+} emissions as a result. The lack of such process in the core/shell NPs, where Er^{3+} and Nd^{3+} were separated in two phases, and, at the same time, detected emission of Nd^{3+} ions when Er^{3+}, Yb^{3+} and Nd^{3+} ions were in one phase, confirmed the successful formation of core/shell NPs via the hydrothermal process. The spectroscopic properties of the synthesized NPs are promising for biomedical applications for deep tissue imaging as the emission can be obtained via excitation within biological windows (808 and 1532 nm), as well as for energy conversion in solar cells where all three excitation wavelengths fall in the range not absorbed by Si-based cells.

Declaration of competing interest

The authors declare that they have no known competing financial interests or personal relationships that could have appeared to influence the work reported in this paper.

CRediT authorship contribution statement

Dominika Przybylska: Conceptualization, Investigation, Writing - original draft, Visualization. **Tomasz Grzyb:** Conceptualization, Resources, Writing - review & editing, Visualization, Supervision.

Acknowledgements

Funding for this research was provided by the National Science Centre, Poland, under grants 2016/21/B/ST8/00477, 2016/22/E/ST5/00016 and 2017/27/N/ST5/02149.

Appendix A. Supplementary data

Supplementary data to this article can be found online at https://doi.org/10.1016/j.jallcom.2020.154797.

References

[1] N. Bloembergen, Solid state infrared quantum counters, Phys. Rev. Lett. 2 (1959) 84–85, https://doi.org/10.1103/PhysRevLett.2.84.

[2] F. Auzel, Compteur quantique par transfert d'energie entre de Yb^{3+} a Tm^{3+} dans un tungstate mixte et dans verre germanate, C. R. Acad. Sci. Paris B. 263 (1966) 819–821.

[3] F. Wang, D. Banerjee, Y. Liu, X. Chen, X. Liu, Upconversion nanoparticles in biological labeling, imaging, and therapy, Analyst 135 (2010) 1839–1854, https://doi.org/10.1039/c0an00144a.

[4] Y. Il Park, H.M. Kim, J.H. Kim, K.C. Moon, B. Yoo, K.T. Lee, N. Lee, Y. Choi, W. Park, D. Ling, K. Na, W.K. Moon, S.H. Choi, H.S. Park, S.-Y. Yoon, Y.D. Suh, S.H. Lee, T. Hyeon, Theranostic probe based on lanthanide-doped nanoparticles for simultaneous in vivo dual-modal imaging and photodynamic therapy, Adv. Mater. 24 (2012) 5755–5761, https://doi.org/10.1002/adma.201202433.

[5] S. Wang, J. Feng, S. Song, H. Zhang, Rare earth fluorides upconversion nanophosphors: from synthesis to applications in bioimaging, CrystEngComm 15 (2013) 7142, https://doi.org/10.1039/c3ce40679b.

[6] D. Tu, Y. Liu, H. Zhu, X. Chen, Optical/magnetic multimodal bioprobes based on lanthanide-doped inorganic nanocrystals, Chem. Eur J. 19 (2013) 5516–5527, https://doi.org/10.1002/chem.201204640.

[7] G. Chen, H. Qiu, P.N. Prasad, X. Chen, Upconversion nanoparticles: design, nanochemistry, and applications in theranostics, Chem. Rev. 114 (2014) 5161–5214, https://doi.org/10.1021/cr400425h.

[8] L.-D. Sun, Y.-F. Wang, C.-H. Yan, Paradigms and challenges for bioapplication of rare earth upconversion luminescent nanoparticles: small size and tunable emission/excitation spectra, Acc. Chem. Res. 47 (2014) 1001–1009, https://doi.org/10.1021/ar400218t.

[9] A. Rapaport, J. Milliez, M. Bass, A. Cassanho, H. Jenssen, Review of the properties of Up-conversion phosphors for new emissive displays, IEEE/OSA J. Disp. Technol. 2 (2006) 68–78, https://doi.org/10.1109/JDT.2005.863781.

[10] T.R. Hinklin, S.C. Rand, R.M. Laine, Transparent, polycrystalline upconverting nanoceramics: towards 3-D displays, Adv. Mater. 20 (2008) 1270–1273, https://doi.org/10.1002/adma.200701235.

[11] W.G. van Sark, J. de Wild, J.K. Rath, A. Meijerink, R.E. Schropp, Upconversion in solar cells, Nanoscale Res. Lett. 8 (2013) 81, https://doi.org/10.1186/1556-276X-8-81.

[12] B.M. van der Ende, L. Aarts, A. Meijerink, Lanthanide ions as spectral converters for solar cells, Phys. Chem. Chem. Phys. 11 (2009) 11081, https://doi.org/10.1039/b913877c.

[13] R. Ma, R. Shimmon, A. McDonagh, P. Maynard, C. Lennard, C. Roux, Fingermark detection on non-porous and semi-porous surfaces using YVO_4:Er,Yb luminescent upconverting particles, Forensic Sci. Int. 217 (2012) e23–e26, https://doi.org/10.1016/j.forsciint.2011.10.033.

[14] C.M. Liu, L.Y. Zhang, L. Li, B.Y. Li, C.G. Wang, T.T. Wang, Specific detection of latent human blood fingerprints using antibody modified $NaYF_4$:Yb,Er,Gd fluorescent upconversion nanorods, Dyes Pigments 149 (2018) 822–829, https://doi.org/10.1016/j.dyepig.2017.11.050.

[15] M. Runowski, J.J. Marciniak, T. Grzyb, D. Przybylska, A. Shyichuk, B. Barszcz, A. Katrusiak, S. Lis, Lifetime nanomanometry - high-pressure luminescence of up-converting lanthanide nanocrystals - SrF_2:Yb^{3+},Er^{3+}, Nanoscale 9 (2017) 16030–16037, https://doi.org/10.1039/C7NR04353H.

[16] F. Auzel, Upconversion and anti-Stokes processes with f and d ions in solids, Chem. Rev. 104 (2004) 139–173, https://doi.org/10.1021/cr020357g.

[17] J. Chen, J.X. Zhao, Upconversion nanomaterials: synthesis, mechanism, and applications in sensing, Sensors 12 (2012) 2414–2435, https://doi.org/10.3390/s120302414.

[18] V. Mahalingam, J. Thirumalai, R. Krishnan, S. Mantha, Up/down conversion luminescence and charge compensation investigation of $Ca_{0.5}Y_{1-x}(WO_4)_2$:xLn^{3+} (Ln = Pr, Sm, Eu, Tb, Dy, Yb/Er) phosphors, Spectrochim. Acta Part A Mol. Biomol. Spectrosc. 152 (2016) 172–180, https://doi.org/10.1016/j.saa.2015.06.129.

[19] J.-C.G. Bünzli, C. Piguet, Taking advantage of luminescent lanthanide ions, Chem. Soc. Rev. 34 (2005) 1048–1077, https://doi.org/10.1039/b406082m.

[20] L. Cheng, C. Wang, Z. Liu, Upconversion nanoparticles and their composite nanostructures for biomedical imaging and cancer therapy, Nanoscale 5 (2013) 23–37, https://doi.org/10.1039/C2NR32311G.

[21] M.Z. Huang, B. Yuan, L. Dai, M.L. Fu, Toward NIR driven photocatalyst: fabrication, characterization, and photocatalytic activity of β-$NaYF_4$:Yb^{3+},Tm^{3+}/g-C_3N_4 nanocomposite, J. Colloid Interface Sci. 460 (2015) 264–272, https://doi.org/10.1016/j.jcis.2015.08.063.

[22] Z. Xue, X. Li, Y. Li, M. Jiang, G. Ren, H. Liu, S. Zeng, J. Hao, A 980 nm laser-activated upconverted persistent probe for NIR-to-NIR rechargeable in vivo bioimaging, Nanoscale 9 (2017) 7276–7283, https://doi.org/10.1039/C6NR09716B.

[23] M.V. DaCosta, S. Doughan, Y. Han, U.J. Krull, Lanthanide upconversion nanoparticles and applications in bioassays and bioimaging: a review, Anal. Chim. Acta 832 (2014) 1–33, https://doi.org/10.1016/j.aca.2014.04.030.

[24] M.H. Alkahtani, C.L. Gomes, P.R. Hemmer, Engineering water-tolerant core/shell upconversion nanoparticles for optical temperature sensing, Opt. Lett. 42 (2017) 2451, https://doi.org/10.1364/OL.42.002451.

[25] Y.-F. Wang, G.-Y. Liu, L.-D. Sun, J.-W. Xiao, J.-C. Zhou, C.-H. Yan, Nd^{3+}-sensitized upconversion nanophosphors: efficient in vivo bioimaging probes with minimized heating effect, ACS Nano 7 (2013) 7200–7206, https://doi.org/10.1021/nn402601d.

[26] B. Liu, C. Li, P. Yang, Z. Hou, J. Lin, 808-nm-Light-Excited lanthanide-doped nanoparticles: rational design, luminescence control and theranostic applications, Adv. Mater. 29 (2017), https://doi.org/10.1002/adma.201605434.

[27] A. Hong, Y. Kim, T.S. Lee, S. Kim, K. Lee, G. Kim, H.S. Jang, Intense red-emitting upconversion nanophosphors (800 nm-driven) with a core/double-shell structure for dual-modal upconversion luminescence and magnetic resonance in vivo imaging applications, ACS Appl. Mater. Interfaces 10 (2018) 12331–12340, https://doi.org/10.1021/acsami.7b18078.

[28] X. Li, R. Wang, F. Zhang, L. Zhou, D. Shen, C. Yao, D. Zhao, Nd^{3+} sensitized up/down converting dual-mode nanomaterials for efficient in-vitro and in-vivo bioimaging excited at 800 nm, Sci. Rep. 3 (2013) 3536, https://doi.org/10.1038/srep03536.

[29] K. Prorok, M. Pawlyta, W. Stręk, A. Bednarkiewicz, Energy migration up-conversion of Tb^{3+} in Yb^{3+} and Nd^{3+} codoped active-core/active-shell colloidal nanoparticles, Chem. Mater. 28 (2016) 2295–2300, https://doi.org/10.1021/acs.chemmater.6b00353.

[30] X. Xie, N. Gao, R. Deng, Q. Sun, Q. Xu, X. Liu, Mechanistic investigation of photon upconversion in Nd^{3+} -sensitized core–shell nanoparticles, J. Am. Chem. Soc. 135 (2013) 12608–12611, https://doi.org/10.1021/ja4075002.

[31] S. Wen, J. Zhou, K. Zheng, A. Bednarkiewicz, X. Liu, D. Jin, Advances in highly doped upconversion nanoparticles, Nat. Commun. 9 (2018), https://doi.org/10.1038/s41467-018-04813-5.

[32] L. Zeng, D. Wu, G. Lu, Y. Pan, J. Zhang, A. Wu, Y. Tian, Recent progress in 808 nm excited upconversion nanomaterials as multifunctional nanoprobes for visualized theranostics in cancers, Curr. Med. Chem. 25 (2017) 2954–2969, https://doi.org/10.2174/0929867324666170320115959.

[33] X. Zhang, Z. Zhao, X. Zhang, D.B. Cordes, B. Weeks, B. Qiu, K. Madanan, D. Sardar, J. Chaudhuri, Magnetic and optical properties of $NaGdF_4$:Nd^{3+}, Yb^{3+}, Tm^{3+} nanocrystals with upconversion/downconversion luminescence from visible to the near-infrared second window, Nano Res 8 (2015) 636–648, https://doi.org/10.1007/s12274-014-0548-2.

[34] K. Wang, W. Qincheng, Y. Zhang, R. Qiao, S. Li, Z. Li, Synthesis of Nd^{3+}/Yb^{3+} sensitized upconversion core–shell nanocrystals with optimized hosts and doping concentrations, RSC Adv. 5 (2015) 62899–62904, https://doi.org/10.1039/C5RA09873D.

[35] M. Pokhrel, C. Valdes, Y. Mao, Ultraviolet upconversion enhancement in triply doped $NaYF_4$:Tm^{3+}, Yb^{3+} particles: the role of Nd^{3+} or Gd^{3+} Co-doping, Opt. Mater. 58 (2016) 67–75, https://doi.org/10.1016/j.optmat.2016.05.020.

[36] L. Tian, Z. Xu, S. Zhao, Y. Cui, Z. Liang, J. Zhang, X. Xu, The upconversion luminescence of Er^{3+}/Yb^{3+}/Nd^{3+} triply-doped β-$NaYF_4$ nanocrystals under 808-nm excitation, Materials 7 (2014) 7289–7303, https://doi.org/10.3390/ma7117289.

[37] J. Xu, M. Sun, Y. Kuang, H. Bi, B. Liu, D. Yang, R. Lv, S. Gai, F. He, P. Yang, Markedly enhanced up-conversion luminescence by combining IR-808 dye sensitization and core–shell–shell structures, Dalton Trans. 46 (2017) 1495–1501, https://doi.org/10.1039/C6DT04529D.

[38] Y. Qin, Z. Dong, D. Zhou, Y. Yang, X. Xu, J. Qiu, Modification on populating paths of β-$NaYF_4$:Nd/Yb/Ho@SiO_2@Ag core/double-shell nanocomposites with plasmon enhanced upconversion emission, Opt. Mater. Express 6 (2016) 1942, https://doi.org/10.1364/ome.6.001942.

[39] S. Fischer, N.D. Bronstein, J.K. Swabeck, E.M. Chan, A.P. Alivisatos, Precise tuning of surface quenching for luminescence enhancement in core-shell lanthanide-doped nanocrystals, Nano Lett. 16 (2016) 7241–7247, https://doi.org/10.1021/acs.nanolett.6b03683.

[40] X. Yin, H. Wang, Y. Tian, M. Xing, Y. Fu, X. Luo, Three primary color emissions from single multilayered nanocrystals, Nanoscale 10 (2018) 9673–9678, https://doi.org/10.1039/c8nr01752b.

[41] Y. Zhang, X. Liu, Y. Lang, Z. Yuan, D. Zhao, G. Qin, W. Qin, Synthesis of ultrasmall $BaLuF_5$:Yb^{3+},Er^{3+}@$BaLuF_5$:Yb^{3+} active-core–active-shell nanoparticles with enhanced up-conversion and down-conversion luminescence by a layer-by-layer strategy, J. Mater. Chem. C. 3 (2015) 2045–2053, https://doi.org/10.1039/C4TC02541E.

[42] X. Wang, J. Zhuang, Q. Peng, Y. Li, A general strategy for nanocrystal synthesis, Nature 437 (2005) 121–124, https://doi.org/10.1038/nature03968.

[43] Y. Chen, B. Liu, X. Deng, S. Huang, Z. Hou, C. Li, J. Lin, Multifunctional Nd^{3+} -sensitized upconversion nanomaterials for synchronous tumor diagnosis and treatment, Nanoscale 7 (2015) 8574–8583, https://doi.org/10.1039/C5NR00829H.

[44] M. Xia, D. Zhou, Y. Yang, Z. Yang, J. Qiu, Synthesis of ultrasmall hexagonal $NaGdF_4$: Yb^{3+},Er^{3+}@$NaGdF_4$:Yb^{3+}@$NaGdF_4$:Nd^{3+} active-core/active-shell/active-shell nanoparticles with enhanced upconversion lumines, ECS J. Solid State Sci. Technol. 6 (2017) R41–R46, https://doi.org/10.1149/2.0031704jss.

[45] B. Liu, Y. Chen, C. Li, F. He, Z. Hou, S. Huang, H. Zhu, X. Chen, J. Lin, Poly(Acrylic acid) modification of Nd^{3+} -sensitized upconversion nanophosphors for highly efficient UCL imaging and pH-responsive drug delivery, Adv. Funct. Mater. 25 (2015) 4717–4729, https://doi.org/10.1002/adfm.201501582.

[46] B. Chen, F. Wang, $NaYbF_4$@CaF_2 core-satellite upconversion nanoparticles: one-pot synthesis and sensitive detection of glutathione, Nanoscale 10 (2018) 19898–19905, https://doi.org/10.1039/c8nr05552a.

[47] X. Chen, D. Peng, Q. Ju, F. Wang, Photon upconversion in core-shell nanoparticles, Chem. Soc. Rev. 44 (2014) 1318–1330, https://doi.org/10.1039/c4cs00151f.

[48] L. Lei, S. Xu, J. Yang, H.W.H. Lee, Power-dependent optical property of Yb/Er:

$NaGdF_4$ @Yb:$NaGdF_4$@Yb:$NaNdF_4$ nanocrystals, Nano 12 (2017) 1750086, https://doi.org/10.1142/S1793292017500862.
[49] D. Wang, B. Xue, J. Song, J. Qu, Compressed energy transfer distance for remarkable enhancement of the luminescence of Nd^{3+}-sensitized upconversion nanoparticles, J. Mater. Chem. C. 6 (2018) 6597–6604, https://doi.org/10.1039/c8tc00936h.
[50] Z. Xia, P. Du, L. Liao, Facile hydrothermal synthesis and upconversion luminescence of tetragonal Sr_2LnF_7:Yb^{3+}/Er^{3+} (Ln = Y, Gd) nanocrystals, Phys. Status Solidi Appl. Mater. Sci. 210 (2013) 1734–1737, https://doi.org/10.1002/pssa.201329114.
[51] J. Sun, J. Xian, H. Du, Hydrothermal synthesis of $BaYF_5$:Yb^{3+}/Er^{3+} upconversion luminescence submicrospheres by a surfactant-free aqueous solution route, J. Phys. Chem. Solid. 72 (2011) 207–213, https://doi.org/10.1016/j.jpcs.2010.12.013.
[52] A. Szczeszak, T. Grzyb, B. Barszcz, V. Nagirnyi, A. Kotlov, S. Lis, Hydrothermal synthesis and structural and spectroscopic properties of the new triclinic form of $GdBO_3$:Eu^{3+} nanocrystals, Inorg. Chem. 52 (2013) 4934–4940, https://doi.org/10.1021/ic302525k.
[53] T. Grzyb, D. Przybylska, Formation mechanism, structural, and upconversion properties of alkaline rare-earth fluoride nanocrystals doped with Yb^{3+}/Er^{3+} ions, Inorg. Chem. 57 (2018) 6410–6420, https://doi.org/10.1021/acs.inorgchem.8b00484.
[54] M. Wang, G. Abbineni, A. Clevenger, C. Mao, S. Xu, Upconversion nanoparticles: synthesis, surface modification and biological applications, Nanomed. Nanotechnol. Biol. Med. 7 (2011) 710–729, https://doi.org/10.1016/j.nano.2011.02.013.
[55] T. Jiang, W. Qin, J. Zhou, Citric acid-assisted phase controlled synthesis of $NaYF_4$:Yb^{3+},Tm^{3+} crystals and their intense ultraviolet upconversion emissions, J. Fluor. Chem. 156 (2013) 177–182, https://doi.org/10.1016/j.jfluchem.2013.10.007.
[56] T. Grzyb, S. Balabhadra, D. Przybylska, M. Węcławiak, Upconversion luminescence in $BaYF_5$, $BaGdF_5$ and $BaLuF_5$ nanocrystals doped with Yb^{3+}/Ho^{3+}, Yb^{3+}/Er^{3+} or Yb^{3+}/Tm^{3+} ions, J. Alloys Compd. 649 (2015) 606–616, https://doi.org/10.1016/j.jallcom.2015.07.151.
[57] S. Zanzoni, M. Pedroni, M. D'Onofrio, A. Speghini, M. Assfalg, Paramagnetic nanoparticles leave their mark on nuclear spins of transiently adsorbed proteins, J. Am. Chem. Soc. 138 (2016) 72–75, https://doi.org/10.1021/jacs.5b11582.
[58] A.-H.H. Li, M. Lü, J. Yang, L. Chen, X. Cui, Z. Sun, Upconversion-luminescent/magnetic dual-functional sub-20 nm core-shell SrF_2:Yb,Tm@CaF_2:Gd heteronanoparticles, Dalton Trans. 45 (2016) 5800–5807, https://doi.org/10.1039/c6dt00237d.
[59] P. Cortelletti, A. Skripka, C. Facciotti, M. Pedroni, G. Caputo, N. Pinna, M. Quintanilla, A. Benayas, F. Vetrone, A. Speghini, Tuning the sensitivity of lanthanide-activated NIR nanothermometers in the biological windows, Nanoscale 10 (2018) 2568–2576, https://doi.org/10.1039/c7nr06141b.
[60] A.M. Pak, J.A. Ermakova, S.V. Kuznetsov, A.V. Ryabova, D.V. Pominova, V.V. Voronov, Efficient visible range SrF_2:Yb:Er- and SrF_2:Yb:Tm-based upconversion luminophores, J. Fluor. Chem. 194 (2017) 16–22, https://doi.org/10.1016/j.jfluchem.2016.12.002.
[61] Z. Zhou, W. Li, J. Song, G. Yi, B. Mei, L. Su, Synthesis and characterization of Nd^{3+} doped SrF_2 nanoparticles prepared by precipitation method, Ceram. Int. 44 (2018) 4344–4350, https://doi.org/10.1016/j.ceramint.2017.12.028.
[62] M. Pedroni, F. Piccinelli, T. Passuello, S. Polizzi, J. Ueda, P. Haro-González, L. Martinez Maestro, D. Jaque, J. García-Solé, M. Bettinelli, A. Speghini, Water (H_2O and D_2O) dispersible NIR-to-NIR upconverting Yb^{3+}/Tm^{3+} doped MF_2 (M = Ca, Sr) colloids: influence of the host crystal, Cryst. Growth Des. 13 (2013) 4906–4913, https://doi.org/10.1021/cg401077v.
[63] S. Kuznetsov, Y. Ermakova, V. Voronov, P. Fedorov, D. Busko, I.A. Howard, B.S. Richards, A. Turshatov, Up-conversion quantum yields of SrF_2:Yb^{3+},Er^{3+} sub-micron particles prepared by precipitation from aqueous solution, J. Mater. Chem. C 6 (2018) 598–604, https://doi.org/10.1039/C7TC04913G.
[64] Z. Huang, H. Gao, Y. Mao, Understanding the effect of Mn^{2+} on Yb^{3+}/Er^{3+}upconversion and obtaining a maximum upconversion fluorescence enhancement in inert-core/active-shell/inert-shell structures, RSC Adv. 6 (2016) 83321–83327, https://doi.org/10.1039/c6ra10969a.
[65] S. Yu, Z. Wang, R. Cao, L. Meng, Microwave–assisted synthesis of water–disperse and biocompatible $NaGdF_4$:Yb,Ln@$NaGdF_4$ nanocrystals for UCL/CT/MR multimodal imaging, J. Fluor. Chem. 200 (2017) 77–83, https://doi.org/10.1016/j.jfluchem.2017.06.002.
[66] T. Jiang, W. Qin, W. Di, R. Yang, D. Liu, X. Zhai, G. Qin, Citric acid-assisted hydrothermal synthesis of α-$NaYF_4$:Yb^{3+},Tm^{3+} nanocrystals and their enhanced ultraviolet upconversion emissions, CrystEngComm 14 (2012) 2302, https://doi.org/10.1039/c2ce06311e.
[67] F. He, P. Yang, D. Wang, N. Niu, S. Gai, X. Li, Self-assembled β-$NaGdF_4$ microcrystals: hydrothermal synthesis, morphology evolution, and luminescence properties, Inorg. Chem. 50 (2011) 4116–4124, https://doi.org/10.1021/ic200155q.
[68] A. Bartkowiak, A. Siejca, K. Borkowski, S. Lis, T. Grzyb, Up-converting LuF_3 and $NaLuF_4$ fluorides doped with Yb^{3+}/Er^{3+} or Yb^{3+}/Tm^{3+} ions for latent fingermarks detection, J. Alloys Compd. 784 (2019) 641–652, https://doi.org/10.1016/j.jallcom.2018.12.344.
[69] R.D. Shannon, Revised effective ionic radii and systematic studies of interatomic distances in halides and chalcogenides, Acta Crystallogr. A. 32 (1976) 751–767, https://doi.org/10.1107/S0567739476001551.
[70] P. Scherrer, Bestimmung der Grösse und der inneren Struktur von Kolloidteilchen mittels Röntgenstrahlen, Nachr. Ges. Wiss. Göttingen. 26 (1918) 98–100.
[71] Y. Wang, L. Ji, B. Zhang, P. Yin, Y. Qiu, D. Song, J. Zhou, Q. Li, Upconverting rare-earth nanoparticles with a paramagnetic lanthanide complex shell for upconversion fluorescent and magnetic resonance dual-modality imaging, Nanotechnology 24 (2013), https://doi.org/10.1088/0957-4484/24/17/175101.
[72] K. Prorok, M. Pawlyta, W. Stręk, A. Bednarkiewicz, Energy migration upconversion of Tb^{3+} in Yb^{3+} and Nd^{3+} codoped active-core/active-shell colloidal nanoparticles, Chem. Mater. 28 (2016) 2295–2300, https://doi.org/10.1021/acs.chemmater.6b00353.
[73] I. Villa, A. Vedda, I.X. Cantarelli, M. Pedroni, F. Piccinelli, M. Bettinelli, A. Speghini, M. Quintanilla, F. Vetrone, U. Rocha, C. Jacinto, E. Carrasco, F.S. Rodríguez, Á. Juarranz, B. del Rosal, D.H. Ortgies, P.H. Gonzalez, J.G. Solé, D.J. García, 1.3 μm emitting SrF_2:Nd^{3+} nanoparticles for high contrast in vivo imaging in the second biological window, Nano Res 8 (2015) 649–665, https://doi.org/10.1007/s12274-014-0549-1.
[74] Y. Zhang, F. Wang, Y. Lang, J. Yin, M. Zhang, X. Liu, D. Zhang, D. Zhao, G. Qin, W. Qin, $KMnF_3$:Yb^{3+},Er^{3+}@$KMnF_3$:Yb^{3+} active-core-active-shell nanoparticles with enhanced red up-conversion fluorescence for polymer-based waveguide amplifiers operating at 650 nm, J. Mater. Chem. C. 3 (2015) 9827–9832, https://doi.org/10.1039/c5tc01838b.
[75] Q. Luo, X. Deng, W. Chen, H. Guo, W. Ou-Yang, X. Chen, S. Huang, Enhancing upconversion from $NaYF_4$:Yb,Er@$NaYF_4$ core–shell nanoparticles assembled on metallic nanostructures, J. Nanosci. Nanotechnol. 18 (2017) 5063–5073, https://doi.org/10.1166/jnn.2018.15355.
[76] M. Pollnau, D. Gamelin, S. Lüthi, H. Güdel, M. Hehlen, Power dependence of upconversion luminescence in lanthanide and transition-metal-ion systems, Phys. Rev. B 61 (2000) 3337–3346, https://doi.org/10.1103/PhysRevB.61.3337.
[77] Y. Zhong, G. Tian, Z. Gu, Y. Yang, L. Gu, Y. Zhao, Y. Ma, J. Yao, Elimination of photon quenching by a transition layer to fabricate a quenching-shield sandwich structure for 800 nm excited upconversion luminescence of Nd^{3+}-sensitized nanoparticles, Adv. Mater. 26 (2014) 2831–2837.
[78] F. Wang, R. Deng, J. Wang, Q. Wang, Y. Han, H. Zhu, X. Chen, X. Liu, Tuning upconversion through energy migration in core-shell nanoparticles, Nat. Mater. 10 (2011) 968–973, https://doi.org/10.1038/nmat3149.